# Model Assessment of the Ability of MODIS to Measure Top-of-Atmosphere Direct Radiative Forcing from Smoke Aerosols

LORRAINE A. REMER AND YORAM J. KAUFMAN

*Laboratory for Atmospheres, NASA Goddard Space Flight Center, Greenbelt, Maryland*

ZEV LEVIN

*Department of Geophysics and Planetary Sciences, Tel Aviv University, Ramat Aviv, Israel*

STEVEN GHAN

*Pacific Northwest Laboratory, Richland, Washington*

ABSTRACT

The new generation of satellite sensors such as the moderate resolution imaging spectroradiometer (MODIS) will be able to detect and characterize global aerosols with an unprecedented accuracy. The question remains whether this accuracy will be sufficient to narrow the uncertainties in estimates of aerosol radiative forcing at the top of the atmosphere. The discussion is narrowed to cloud-free direct forcing. Satellite remote sensing detects aerosol with the least amount of relative error when aerosol loading is high. Satellites are less effective when aerosol loading is low. The monthly mean results of two global aerosol transport models are used to simulate the spatial distribution of smoke aerosol in the Southern Hemisphere during the tropical biomass burning season. This spatial distribution allows us to determine that 87%–94% of the smoke aerosol forcing at the top of the atmosphere occurs in grid squares with sufficient signal-to-noise ratio to be detectable from space. The uncertainty of quantifying the smoke aerosol forcing in the Southern Hemisphere depends on the uncertainty introduced by errors in estimating the background aerosol, errors resulting from uncertainties in surface properties, and errors resulting from uncertainties in assumptions of aerosol properties. These three errors combine to give overall uncertainties of 1.2 to 2.2 W m$^{-2}$ (16%–60%) in determining the Southern Hemisphere smoke aerosol forcing at the top of the atmosphere. Residual cloud contamination uncertainty is not included in these estimates. Strategies that use the satellite data to derive flux directly or use the data in conjunction with ground-based remote sensing and aerosol transport models can reduce these uncertainties.

## 1. Introduction

The role of aerosol forcing remains one of the largest uncertainties in estimates of man's impact on the global climate system (Houghton and Ding 2001). Man-made aerosols may cool the earth directly by scattering radiation back to space (Charlson et al. 1992; Lacis and Mischenko 1995). They may cool the earth indirectly by increasing the number of cloud condensation nuclei in clouds, and thereby increasing the number of cloud droplets and the reflectance back to space (Twomey 1977). Man-made aerosols may also influence the radiative balance in other ways including absorption of solar radiation and changing atmospheric stability profiles and subsequently cloud formation (Hansen et al.

*Corresponding author address:* Lorraine A. Remer, Laboratory for Atmospheres, NASA Goddard Space Flight Center, Code 913, Greenbelt, MD 20771.
E-mail: remer@climate.gsfc.nasa.gov

1997). Satheesh and Ramanathan (2000), using measurements from the Indian Ocean Experiment, showed that understanding radiative forcing at the top of the atmosphere (TOA) is not enough to represent the aerosol effect on climate. Absorbing aerosol, for example, biomass burning (Martins et al. 1998), regional pollution over the Indian Ocean (Satheesh et al. 1999) and dust (Alpert et al. 1998) can affect atmospheric heating rates, evaporation, and cloud formation; thus affecting climate even without directly changing the energy balance at the top of the atmosphere. However, the TOA energy forcing remains an important unknown quantity in the equation and forms the focus of this paper.

Although much progress has been made in the past decade in terms of characterizing aerosol properties, identifying their extent and determining their role in the radiative balance, too much uncertainty remains to make definitive statements. Narrowing the uncertainty is vital, yet how do we proceed?

One school of thought suggests that remote sensing

by satellite sensors will provide the data necessary to narrow these uncertainties. On the other hand, satellite sensors are not a panacea to the problem. Although the new generation of sensors has excellent accuracy compared to the heritage instruments of the past (Chu et al. 1998; Tanré et al. 1999), they still have measurement limitations (King et al. 1999; Kaufman et al. 1997a; Tanré et al. 1997). In clean, pristine regions the absolute magnitude of the uncertainty in the aerosol retrieval becomes comparable in magnitude to the signal itself.

Much of the important aerosol radiative forcing may occur within the noise level of the accuracy of the remote sensing measurements. Man-made aerosols can be transported far from the source regions (McGovern et al. 1999; Perry et al. 1999). Biomass burning aerosols traced from the continents were observed in the remote southern ocean during Pacific Exploratory Mission-Tropics (Stoller et al. 1999). Although concentrations were dilute, the background aerosol is also of small magnitude. The imported man-made aerosol could effectively double the aerosol loading in remote regions (Stoller et al. 1999), and if over a large enough area, may play a large role in the global aerosol forcing. If much of the aerosol forcing is occurring at very low magnitudes of aerosol concentrations, present satellite remote sensing will miss it.

Another limitation of remote sensing is that satellites see the atmosphere as it is now, not the changes due to human activity. They will measure aerosol that includes both a man-made component (industrial origin, biomass burning origin) and a natural component (desert dust, sea salt). Remote sensing cannot separate the aerosol measurement into components, except in the coarsest of manners by separating by aerosol size. Knowing the magnitude of the background aerosol signal is a prerequisite before determining the magnitude of the man-made perturbation to the signal, a prerequisite that satellites may not meet.

This study, we hope, is a first step in developing a strategy to best use satellite data to estimate the global aerosol direct forcing. We start with the pair of aerosol retrieval algorithms developed for the Earth Observing System moderate resolution imaging spectrometer (MODIS) instrument (Kaufman et al. 1997a; Tanré et al. 1997), and use the uncertainties inherent in these algorithms as representative of remote sensing in general. To simulate the distribution of aerosol we use simulated data from aerosol transport models. In order to avoid the complications of multiple types of man-made aerosols we turn to the distribution of biomass burning aerosol in the Southern Hemisphere during the season when smoke aerosol dominates the man-made contribution to the aerosol loading.

This study is not an intercomparison of global transport models. It is not an estimation of global aerosol forcing. This study, based on model simulations, is an exercise to determine whether satellite remote sensing can live up to the high expectations surrounding its development.

## 2. Uncertainty of MODIS aerosol retrievals

The MODIS procedure for the remote sensing of aerosol consists of two separate algorithms. One derives aerosol over land (Kaufman et al. 1997a) and makes use of dark targets identified with the mid-IR channels (Kaufman et al. 1997b) and dynamical aerosol models (Remer and Kaufman 1998; Remer et al. 1998; Tanré et al. 2001). The other derives aerosol over the ocean by inverting the multispectral radiance field (Tanré et al. 1997).

In both methods, the retrievals will be affected by errors associated with estimating the surface reflectance, instrument calibration, and assumptions of aerosol properties that are not retrieved in the algorithm. We describe the uncertainties in the retrievals as:

$$\Delta\tau = \pm 0.05 \pm 0.20\tau$$

$$\text{(land; Kaufman et al. 1997a),} \quad \text{and} \quad (1a)$$

$$\Delta\tau = \pm 0.05 \pm 0.05\tau$$

$$\text{(ocean; Tanré et al. 1997),} \quad (1b)$$

where $\tau$ is the aerosol optical thickness and $\Delta\tau$ is the uncertainty. Equations (1) were derived from theoretical sensitivity studies in which a dataset of aerosol characteristics are input into a radiative transfer code then TOA radiances are calculated. These calculated radiances were then used as input in the MODIS retrieval algorithm to see how close the algorithm could return the original aerosol dataset. A variety of aerosol characteristics were tested (Kaufman et al. 1997a; Tanré et al. 1997). The uncertainties in Eqs. (1) pertain to individual retrievals. We refer to Eqs. (1) as ''low'' accuracy.

Figure 1 shows the Southern Hemisphere distribution of retrieval signal-to-noise ratio ($\tau/\Delta\tau$) based on Eqs. (1) and applied to the simulated August monthly mean results of the model of Tegen et al. (1997). Also shown in Fig. 1 is the model-derived August monthly mean smoke optical thickness. We see signal-to-noise ratio is high over the parts of the continents where optical thickness is high and largest in the ocean regions just offshore and downwind of the smoke source regions. However, Fig. 1a shows the large extent of the Southern Hemisphere in which the uncertainty of our retrievals is comparable in magnitude to the magnitude of the signal itself ($\tau/\Delta\tau \sim 1$).

We find that Eqs. (1) can overpredict the error when the retrieval algorithms are applied to actual field conditions. King et al. (1999) report that for the specific examples of urban–industrial pollution over the Atlantic [Tropospheric Aerosol Radiative Forcing Observational Experiment (TARFOX)] and biomass burning smoke
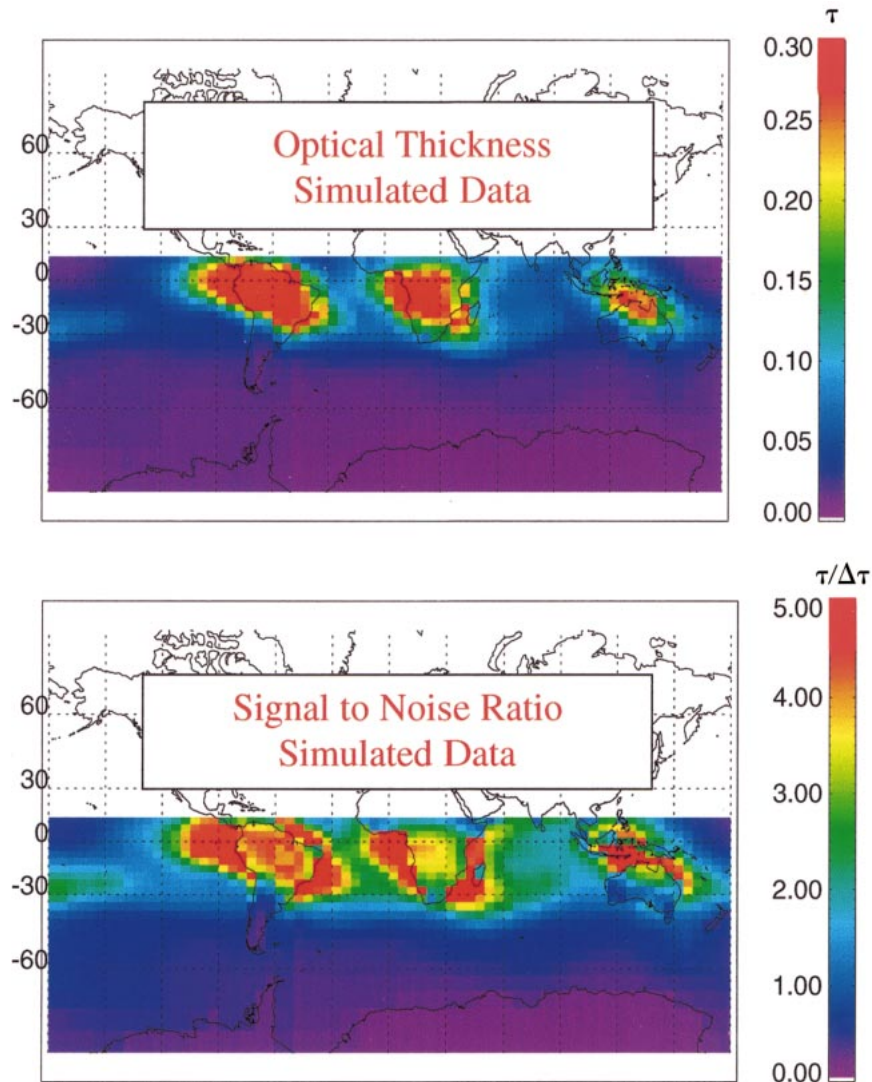
FIG. 1. Southern Hemisphere distribution of simulated Aug monthly mean smoke optical thickness (top) and retrieval signal-to-noise ratio ($\tau/\Delta\tau$) based on Eqs. (1) and applied to the Aug monthly mean results. Data is derived from model 1 (Tegen et al. 1997).

over South America [Smoke, Clouds, and Radiation-Brazil (SCAR-B)] the retrieval errors can be reduced to

$$\Delta\tau = \pm0.05 \pm 0.15\tau \quad \text{(land), and} \quad (2a)$$

$$\Delta\tau = \pm0.01 \pm 0.05\tau \quad \text{(ocean).} \quad (2b)$$

We refer to Eqs. (2) as "high" accuracy. In other situations with different aerosol types and surface backgrounds, errors may be larger than those observed during these specific campaigns. However many of the errors may be random, as shown in the TARFOX and SCAR-B field validations. This creates the possibility that the average value of an ensemble of retrievals will actually be more accurate than Eqs. (1) suggest.

Equations (1) and Eqs. (2) offer two measures of the errors expected from the MODIS retrievals. Equations (1) are a conservative estimate based on theory as applied to individual retrievals. As we see from field experiments in a well-characterized environment, the uncertainties can decrease significantly. Equations (2), based on these field experiments, offer an alternative measure of uncertainty for individual retrievals that may be optimistic, but is certainly achievable in some regions. In other regions it may represent the errors associated with weekly or monthly averages. Preliminary validation of actual MODIS retrievals, using the Aerosol Robotic Network (AERONET) global network as "ground truth" (Holben et al. 1998), suggests that the uncertainty does indeed fall between Eqs. (1) and (2) (Chu et al. 2001, hereafter C01; Ichoku et al. 2001, manuscript submitted to *Geophys. Res. Lett.*, hereafter I01; Remer et al. 2001, hereafter R01). In the following we shall use two aerosol transport models to simulate

the distribution in the Southern Hemisphere of biomass burning aerosol and natural maritime and mineral aerosol. The domain includes all longitudes south of 12°N, as pictured in Fig. 1. Model 1 is given by Tegen et al. (1997) and model 2 by Ghan et al. (2001a–c). We shall use the results to answer the following questions.

- For a given error in the satellite retrieval, what is the fraction of the biomass burning aerosol forcing that is detectable by the satellite (e.g., above a given threshold)?
- How accurately can satellites be used to detect man-made radiative forcing above background aerosol?
- Using the spatial distributions of the aerosol from model 1 and model 2, and the equations for the low and high estimates of the satellite retrievals, what is the overall error in assessing the aerosol forcing (radiative effects above the background)?

## 3. Model and observational data

To simulate the distribution of smoke aerosol in the Southern Hemisphere we turn to the published results of Tegen et al. (1997) (http://gacp.giss.nasa.gov/transport/). The model is based on a general circulation model that generates its own dynamics. It is meant to simulate climatology, not weather. The "weather," day-to-day variation, in the model is too noisy to be meaningful and only monthly mean values are useful. This is different than assimilation models that are driven by input winds and other parameters. Assimilation models may have more accurate day-to-day forecasts but are not practical simulators of climatology. The data consist of monthly mean values of optical thickness distributed over the globe on a 4° × 5° grid and divided by aerosol types that include mineral dust (Tegen and Fung 1995), sea salt (Tegen et al. 1997), sulfate (Chin et al. 1996), and carbonaceous aerosol (Liousse et al. 1996). The carbonaceous aerosol is further divided into organic and black carbon categories. We assume that the sum of organic and black carbon aerosol optical thickness in the Southern Hemisphere represents the optical thickness contribution from biomass burning and are man-made contributions.

Tegen et al. (1997) compare their model results with monthly mean optical thickness measurements taken from AERONET (Holben et al. 1998) radiometers at various global locations. At stations near the source regions of Southern Hemisphere biomass burning, the model appears to severely underestimate the optical thickness. Figure 2 further illustrates the underprediction. The model produces monthly mean values of optical thickness no greater than 0.25, while values 2–7 times larger are observed by the AERONET stations. The model's underprediction is most serious during the height of the biomass burning season in August and September, but also relatively high in October. The model's prediction of optical thickness is fairly accurate in
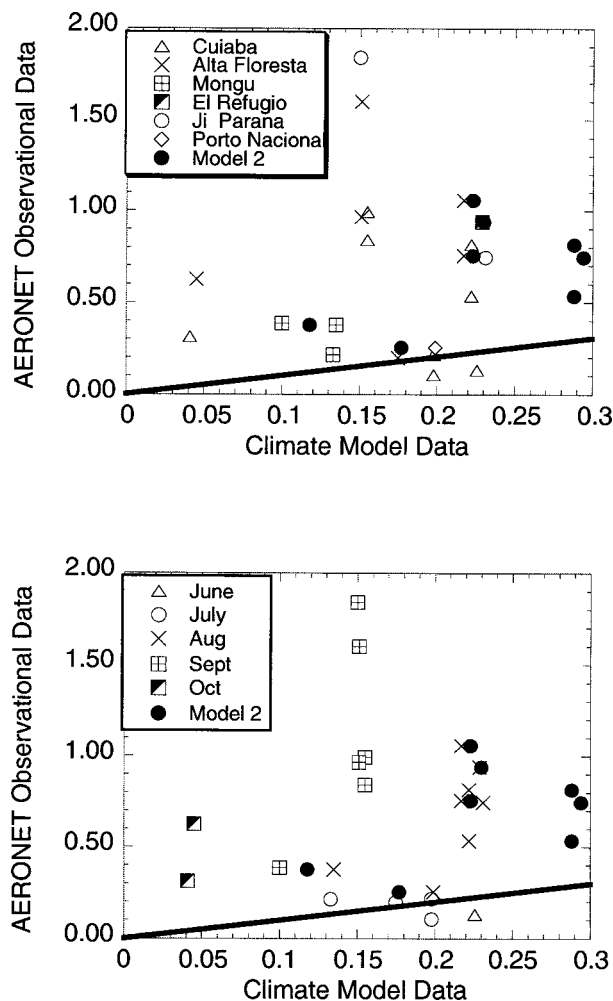


FIG. 2. Comparison of monthly mean values of optical thickness at 550 nm derived from transport model results (Tegen et al. 1997) with values observed by AERONET stations near biomass burning source regions in the Southern Hemisphere. Also shown by black dots are the Aug mean values of model 2 (Ghan et al. 2001a–c) for all the stations. The top figure shows the data grouped by observing station. The bottom figure shows the data grouped by months. Note the different scales on the x and y axes. The solid line represents where the model and observations would be in perfect agreement.

the preburning time period of June and July suggesting that the background aerosol is well-predicted. The under prediction of smoke seems to be worse for the stations in South America and less severe for Mongu, the only African station in this analysis.

Figure 2 also plots August mean values for a second model (Ghan et al. 2001a–c), more fully described in section 7. The two models use similar information to determine source strength, but employ very different aerosol processes and transport mechanisms. The second model also underpredicts smoke optical thickness near sources, in some cases by a strikingly similar amount. The fact that these two very different models both underpredict optical thickness near biomass burn-

ing sources strongly suggest that estimates of source strength is low.

Estimating global source strength of biomass burning is more difficult than estimating where the sources are located or in transporting the aerosol from the source areas. We can identify biomass burning regions using satellite fire counts (Setzer and Pereira 1991; Prins et al. 1998), but quantification of the amount of aerosol emitted must be compiled from production inventories and requires a number of assumptions (Liousse et al. 1996). Furthermore, the global inventories used in the transport model of this study are based on statistics from the 1975–80 period (Liousse et al. 1996; Hao et al. 1990). Emission strengths could certainly have increased from the years the statistical inventories were compiled in the late 1970s to the mid-1990s when the AERONET sun photometer data were acquired.

On the other hand we have no reason to mistrust the model's ability to transport the smoke away from the source regions. Transport in model 1 (Tegen et al. 1997) is provided by the Lagrangian GRANTOUR model and includes transport, transformation and removal of aerosol (Walton et al. 1988). The National Center for Atmospheric Research (NCAR) Community Climate Model provides the wind and precipitation fields. Thus we expect the model well-represents the geographical distribution of smoke aerosol optical thickness, while underestimating the magnitude. In support of this assumption, the spatial pattern of smoke aerosol resembles published distributions from previous satellites (Husar et al. 1997; Herman et al. 1997) and preliminary observations from MODIS (R01). The similarity is apparent despite the fact that the observations are for a particular year while the model is seeking to determine climatological conditions.

To compensate for model 1's underestimation of smoke magnitude, we boost the model-derived smoke optical thickness by multiplicative factors derived from Fig. 2 and specific to month. Only the smoke optical thickness component of the model is boosted. Because Fig. 2 suggests the underestimation is more severe for South America than for Africa, we use two sets of multiplicative factors. For August, the factors are 3.5 for South America and 2.5 for the rest of the world. For September and October, the factors are 8.0 and 4.0, for South America and the remainder of the world, respectively.

## 4. Fraction of the aerosol forcing above a given satellite detection threshold

We use the results of Tegen et al. (1997; model 1) to determine how much of the direct aerosol forcing occurs above the noise levels of the MODIS aerosol retrieval [Eqs. (1) and (2)]. To do so, we calculate histograms of the aerosol optical thickness provided by Tegen et al. (1997). We include only Southern Hemisphere and tropical grid squares, south of latitude 12°N. Before sum-
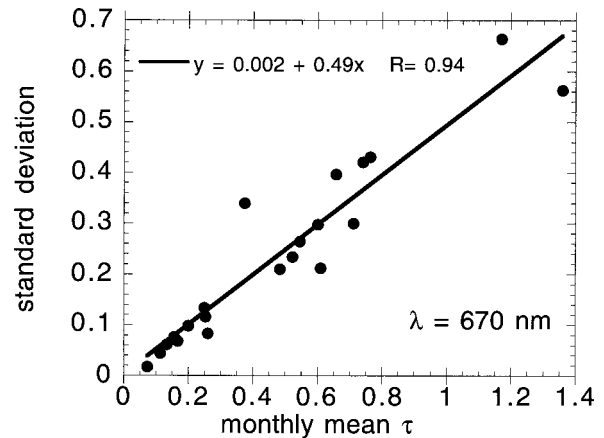


FIG. 3. Std dev about the monthly mean aerosol optical thickness plotted against the monthly mean. The std dev and monthly means are calculated from daily mean values for AERONET stations near biomass burning source regions.

ming the data in the histograms, the monthly mean optical thickness values are adjusted twice. First, by the multiplicative values discussed in section 3 to compensate for the underprediction of smoke sources. Second, is by expanding each monthly mean value into a lognormal distribution with a standard deviation equal to 0.50. The second adjustment is to account for the variability of daily values measured by satellite that are not included in the monthly means. The value of 0.50 for standard deviation was calculated by analyzing several AERONET stations in biomass burning regimes (Fig. 3). A normal distribution gives similar results to the lognormal distribution.

The optical thickness frequency histogram ($f_i$) is defined as

$$f_i = \frac{N_i}{\sum_i N_i},\qquad(3)$$

where the bins are defined as intervals of optical thickness and $N_i$ is the number of area-weighted grid squares in bin $i$. In the single scattering approximation smoke aerosol forcing is directly proportional to $\tau$ (Penner et al. 1992; Hobbs et al. 1997). Although smoke can be too thick near source regions for the single scattering approximation to hold, for most of the domain the smoke is sufficiently thin. The regions of high smoke loading are obviously well above the satellite detection threshold, and the simplification is sufficient to calculate cumulative histograms. Thus, the histogram representing smoke aerosol forcing ($F_i$) will be given by

$$F_i = \frac{\tau_i f_i}{\sum_i \tau_i f_i},\qquad(4)$$

where $\tau_i$ is the optical thickness in bin $i$.

The difference between Eqs. (3) and (4) is that Eq. (4) gives greater weight to grid squares with higher
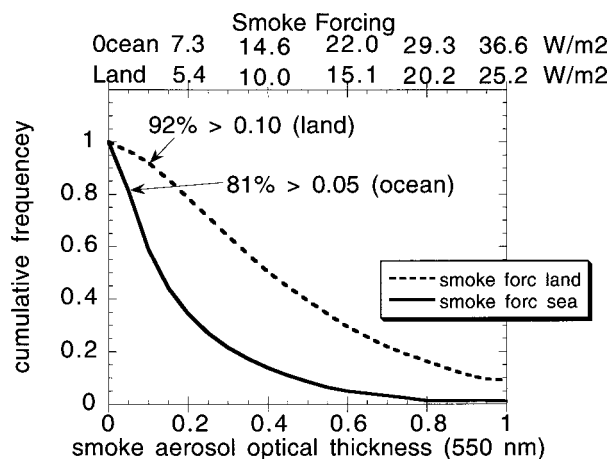
FIG. 4. Cumulative histogram of the smoke aerosol forcing in the Southern Hemisphere for Aug as function of aerosol optical thickness and divided into land and ocean components. Values of smoke direct radiative forcing following Hobbs et al. (1997) and corresponding to the aerosol optical thickness bins, are shown along the top. Arrows indicate percentage of smoke forcing occurring in grid squares above specified smoke aerosol optical thickness thresholds. Histograms calculated from Tegen et al. (1997) data.

optical thickness. Because smoke forcing is proportional to optical thickness, the grid squares at higher optical thickness will contribute proportionally more to the hemispheric smoke forcing. Thus, we rely on Eq. (4), the *weighted* histogram, to calculate smoke forcing. The constant of proportionality that relates optical thickness to forcing cancels in the formulation of Eq. (4). Additional details on the Penner et al. (1992) and Hobbs et al. (1997) approximation and the values of the constant of proportionality are given in section 6.

Figure 4 is a cumulative histogram of the smoke aerosol forcing in the Southern Hemisphere divided into land and ocean components. If we conservatively take noise thresholds for the smoke optical thickness of $\tau = 0.05$ over ocean and $\tau = 0.10$ over land and assume background aerosol can be well-estimated, then 81% of the smoke forcing over ocean and 92% over land will be above noise levels. Because the land represents 20% of the area of our domain but 43% of the smoke forcing (area weighted by $\tau$), 86% of the smoke forcing in the Southern Hemisphere will be detectable by the MODIS algorithms.

## 5. Estimating background conditions from satellite

Satellites see the atmosphere as it is now. Remote sensing will measure the total aerosol consisting of both the natural aerosol and the aerosol due to human activity. Remote sensing cannot effectively determine the man-made component of the aerosol optical thickness without assuming a value for the "background" optical thickness and subtracting the background component from the total. Estimating the background or natural aerosol component introduces much of the error in using

satellites to determine the global aerosol forcing by human activity. We attempt to quantify the uncertainty in making this estimate of background conditions.

One method to estimate background conditions during the biomass burning season is to observe total aerosol optical thickness from satellite in a month with *no* burning, and designate these conditions as background in a month *with* burning. We can test the uncertainty in this method by using the Tegen et al. (1997) results. The background aerosol in the Tegen et al. (1997) results for August is the sum of the nonsmoke categories of aerosol (dust + salt + sulfates). Which month's total aerosol optical thickness (dust + salt + sulfates + smoke) best represents the nonsmoke aerosol optical thickness of August? We test this month by month in an rmse sense for every model grid box, for all latitudes south of 12°N. The results indicate that the minimum difference between monthly mean total aerosol optical thickness and August background aerosol occurs for the month of May with an rmse of 0.027 in optical thickness units.

Other methods of estimating background aerosol that include information from ground-based sensors and other auxiliary data can improve our estimates. For example, AERONET data taken from background marine stations show a very consistent lower envelope aerosol optical thickness (Kaufman et al. 2001). These data suggest that we can make estimates of background aerosol optical thickness to within 0.01 or less. We will use the value of 0.027 as an upper bound and the AERONET-assisted value of 0.01 as a lower bound on the uncertainty associated with estimating the magnitude of the background aerosol.

## 6. Estimate of the error in satellite sensing of aerosol radiative forcing.

We examine error introduced into the aerosol retrieval algorithm from four sources.

1) The uncertainty in estimating background aerosol optical thickness: we will use the value of ±0.027 as an upper bound and ±0.01 as a lower bound, as discussed in section 5.
2) The uncertainty in estimating surface reflectance: this appears mainly as the offset in Eqs. (1) and (2), although depending on geometry there is some $\tau$ dependence. We will use the theoretical values of $\Delta\tau = \pm0.05$ due to uncertainty in the surface reflectance for both land and ocean as a conservative upper bound, as discussed in section 2. We will also use the low value of $\Delta\tau = \pm0.01$ for over the ocean as discussed in section 2.
3) The uncertainty in estimating the aerosol model including the aerosol phase function, refractive index and single scattering albedo.
4) The uncertainty introduced by instrument calibration errors.

TABLE 1. Uncertainty in estimating smoke aerosol forcing in the Southern Hemisphere from MODIS aerosol optical thickness using theoretical estimates of retrieval uncertainty, upper bound of background uncertainty, and model 1.

| | Optical thickness units | | | Radiative flux (W m$^{-2}$) | | | Relative error (%) | | |
|---|---|---|---|---|---|---|---|---|---|
| | Land | Ocean | SH | Land | Ocean | SH | Land | Ocean | SH |
| Background | 0.027 | 0.027 | 0.027 | 0.7 | 1.0 | 0.9 | 13 | 36 | 26 |
| Surface | 0.05 | 0.05 | 0.05 | 1.3 | 1.8 | 1.6 | 23 | 66 | 48 |
| $\tau$-dependent | 0.09 | 0.01 | 0.04 | 2.3 | 0.4 | 1.2 | 42 | 13 | 25 |
| Rmse-combined | 0.11 | 0.06 | 0.07 | 2.7 | 2.1 | 2.1 | 50 | 76 | 60 |

Both error sources (3) and (4) are dependent on the magnitude of the optical thickness. We combine them into one term ($\Delta\tau_i^{\text{dep}}$) and calculate the value from the forcing histograms [Eq. (4)]:

$$\Delta\tau^{\text{dep}} = \sum_i \Delta\tau_i^{\text{dep}} F_i, \qquad (5)$$

where $\Delta\tau_i^{\text{dep}}$ is defined by $\pm 0.05\tau_i$ (ocean) and $\pm 0.20\tau_i$ (land), using theoretical estimates, or $\pm 0.15\tau_i$ for land, using empirical estimates as discussed in section 2. These values are identical to the second terms of Eqs. (1) and (2). Clouds introduce additional uncertainty in the retrievals. Cloud uncertainty is difficult to quantify, and for this study, ignored. Cloud issues are further discussed in section 8.

Table 1 lists the error estimates for the four sources of error with the two $\tau$-dependent sources combined. The different types of errors are combined in the rmse sense. The total Southern Hemisphere values are calculated by weighting the land errors by 43% and the ocean errors by 57% because the land makes up 43% of the smoke aerosol forcing in this August dataset. The first three columns of Table 1 express $\Delta\tau$ in optical thickness units. The analysis suggests that MODIS will determine smoke aerosol forcing in the Southern Hemisphere to within 0.07 in optical thickness units.

Following Penner et al. (1992) smoke aerosol forcing $F$ can be expressed as

$$F = \left[\frac{S}{4}2T^2(1 - A_c)(1 - R_s)^2 B\right]\tau = C\tau, \qquad (6)$$

assuming no absorption. Here, $S$ is the solar flux incident at the top of the atmosphere, $T$ is the atmosphere clear-sky transmittance, $A_c$ is the fraction of clouds, $R_s$ is the surface albedo, $B$ is the fraction of radiation backscattered to space and $\tau$ is the smoke optical thickness. Thus we see that the smoke forcing is directly proportional to $\tau$ and if we assume that all other parameters remain constant, then the uncertainty in smoke aerosol forcing is directly proportional to

$$\Delta F = C\Delta\tau. \qquad (7)$$

Penner et al.'s (1992) values of $C$ are 44 W m$^{-2}$ for ocean and 30 W m$^{-2}$ land. The difference between ocean and land is due to differences in surface albedo. Hobbs et al. (1997) uses different values for the smoke optical properties based on more recent observations, but the

same values for cloud fraction, surface albedo, etc. The Hobbs et al. (1997) values of $C$ are 37 W m$^{-2}$ for ocean and 25 W m$^{-2}$ for land. The middle three columns of Table 1 list the error estimates in units of W m$^{-2}$ after applying Eq. (7) to the uncertainties in optical thickness units and using the Hobbs et al. (1997) values for $C$. The analysis suggests that MODIS remote sensing of aerosol will be able to determine the smoke aerosol forcing in the Southern Hemisphere only to $\pm 2.1$ W m$^{-2}$.

The uncertainty can also be expressed as a relative error given by $\Delta\tau/\tau$:

$$\frac{\Delta\tau}{\tau} = \sum_i \frac{\Delta\tau_i}{\tau_i}F_i = \frac{\sum_i \Delta\tau_i f_i}{\tau_{\text{mean}}}, \qquad (8)$$

where $F_i$ is the forcing histogram [Eq. (4)], $f_i$ the optical thickness histogram [Eq. (3)], $\tau_i$ the optical thickness of the histogram bin, and $\Delta\tau_i$ the uncertainty for $\tau_i$ as given by Eqs. (1) or (2). $\tau_{\text{mean}}$ is defined as

$$\tau_{\text{mean}} = \sum_i \tau_i f_i. \qquad (9)$$

Southern Hemisphere August values for $\tau_{\text{mean}}$ are 0.21 for the land and 0.08 for the ocean. The relative errors given in percentage units are shown in the last three columns of Table 1. In percentage units we see that we can expect to determine smoke aerosol forcing in the Southern Hemisphere to only $\pm 60\%$.

The results in Table 1 are based on theoretical estimates of uncertainty associated with making individual retrievals as applied to the August mean transport model distribution of smoke optical thickness. The largest uncertainty is introduced by errors in determining the surface reflectance, both in an absolute and a relative sense. Substantial error is also introduced in the $\tau$ dependent error over land. As discussed in section 2, field experiment data suggest the theoretical estimates of retrieval uncertainty are conservative and that we may expect improvements in exactly the types of error contributing the greatest values of uncertainty to Table 1. Preliminary validation of the MODIS algorithms also supports a more optimistic view.

Table 2 lists the more optimistic values of expected uncertainty based on empirical estimates [Eqs. (2)]. The results based on Eqs. 2 reduce the uncertainty of estimating smoke forcing in the Southern Hemisphere from $\pm 2.1$ W m$^{-2}$ and $\pm 60\%$ to $\pm 1.2$ W m$^{-2}$ and $\pm 29\%$.

TABLE 2. Uncertainty in estimating smoke aerosol forcing in the Southern Hemisphere from MODIS aerosol optical thickness using empirical estimates of retrieval uncertainty, lower bound of background uncertainty, and model 1.

| | Optical thickness units | | | Radiative flux (W m$^{-2}$) | | | Relative error (%) | | |
|---|---|---|---|---|---|---|---|---|---|
| | Land | Ocean | SH | Land | Ocean | SH | Land | Ocean | SH |
| Background | 0.01 | 0.01 | 0.01 | 0.3 | 0.4 | 0.3 | 5 | 13 | 10 |
| Surface | 0.05 | 0.01 | 0.03 | 1.3 | 0.4 | 0.7 | 23 | 13 | 17 |
| $\tau$-dependent | 0.07 | 0.01 | 0.04 | 1.8 | 0.4 | 0.9 | 33 | 13 | 21 |
| Rmse-combined | 0.09 | 0.02 | 0.05 | 2.2 | 0.6 | 1.2 | 40 | 23 | 29 |

Most of the improvement is due to reducing the errors introduced by uncertainty in the ocean surface reflectance and in estimating background aerosol.

The largest remaining uncertainty is due to errors in the over land algorithm. There is a possibility that in an ensemble of retrievals over different surface types
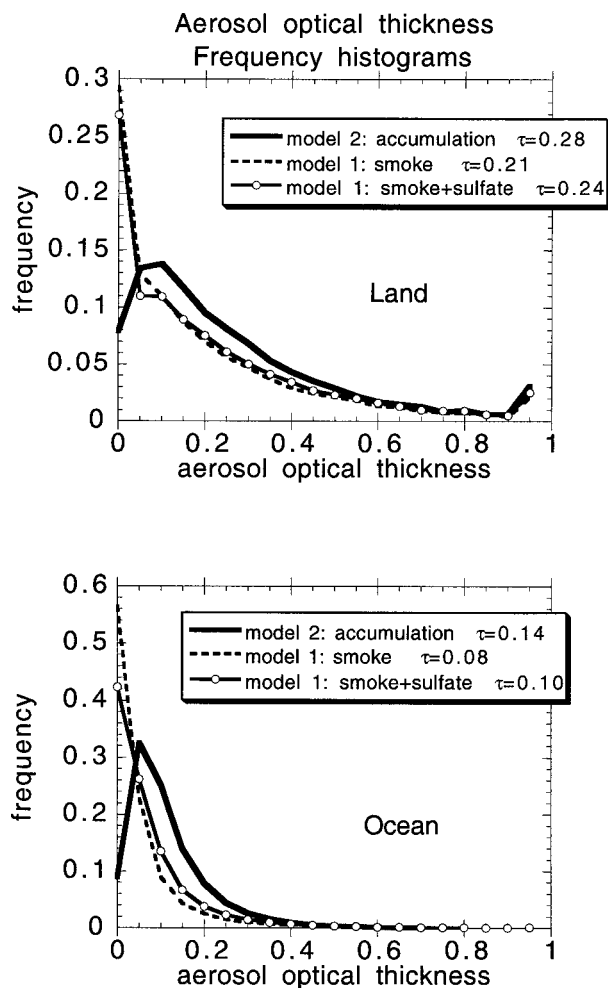


FIG. 5. Aerosol optical thickness frequency histograms over land (top) and ocean (bottom) of the simulated Southern Hemisphere during Aug for two aerosol transport models. Model 1 is Tegen et al. (1997), which separates smoke from sulfate aerosol. Model 2 is Ghan et al. (2001a–c), which combines these two aerosol types into a category labeled accumulation mode. The Southern Hemisphere mean aerosol optical thickness ($\tau$) is given in each category.

the land surface reflectance error may be further reduced.

## 7. Sensitivity to transport model

In the preceding sections a specific aerosol transport model (model 1) reported by Tegen et al. (1997) provided the only distributions of aerosol optical thickness used in the analyses. How sensitive are the preceding estimates of uncertainty to the choice of transport model? We explore this issue by performing a similar analysis using a different model. Model 2 (Ghan et al. 2001a–c) couples a general circulation model with a tropospheric chemistry model becoming a global chemistry model. Models 1 and 2 have independent parameterizations governing aerosol transformation and removal.

One of the major differences between model 1 and model 2 is that model 2 does not separate organic and black carbon aerosol thickness from the total aerosol optical thickness. Model 2 treats a variety of aerosol components in the accumulation mode: sulfate, organic carbon, black carbon, Methane Sulfonic acid (MSA) sea salt, soil dust, and water. In addition, model 2 treats separate coarse dust and sea salt modes. The total aerosol depth is the sum of the accumulation and the two coarse modes. There is also an ultrafine mode, but its contribution is negligible. Because the aerosol components for each mode are assumed to be internally mixed, it is not possible to separate the contributions of each aerosol component to the total optical depth. Smoke aerosol optical thickness is therefore combined with other aerosol types under the category of accumulation-mode aerosol optical thickness. We are forced to assume that accumulation-mode optical thickness in model 2 output is equivalent to smoke optical thickness. By comparing model 2 optical thicknesses in biomass burning source regions with AERONET sun photometer data, we find the same underprediction found when comparing model 1 (Fig. 2) and we adjust the model 2 data by the same multiplicative factors.

Following the same procedure as in section 4, we construct histograms from the model 2 dataset. Figure 5 compares the aerosol optical thickness histograms ($f_i$) of the two transport models. The two models produce different distributions of aerosol optical thickness. Overall, mode 2 produces higher optical thickness in
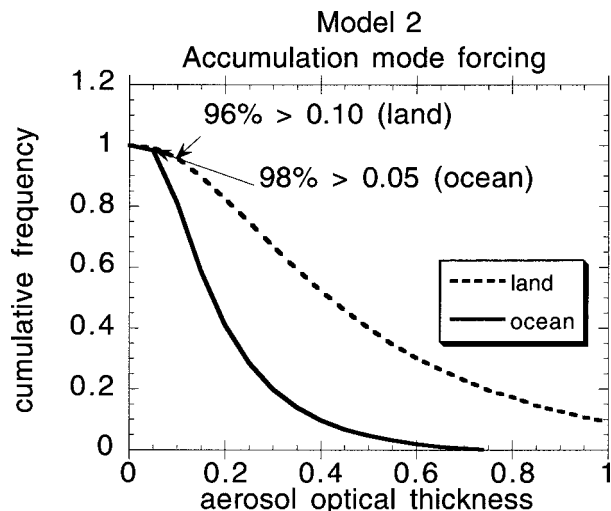
FIG. 6. Model 2 cumulative histogram of the accumulation-mode aerosol forcing in the Southern Hemisphere for Aug as function of the aerosol optical thickness and divided into land and ocean components. Arrows indicate percentage of smoke forcing occurring in grid squares above specified smoke aerosol optical thickness thresholds. Histogram derived from Ghan et al. (2001a–c) simulated data.

the Southern Hemisphere than does model 1. The mean accumulation mode $\tau$ for model 2 is 0.28 over land and 0.14 over ocean. This compares with mean smoke $\tau$ of 0.21 over land and 0.08 over ocean in model 1. However, for a fair comparison we should compare accumulation mode aerosol in both models and combine smoke with sulfate in model 1. The combined accumulation mode aerosol consisting of smoke plus sulfate in model 1 gives mean $\tau$ of only 0.24 over land and 0.10 over ocean. Thus, model 1 and model 2 produce different aerosol optical thickness distributions.

Figure 6 shows the cumulative histogram constructed from model 2 output. Virtually all the data exceed the threshold values of $\tau = 0.10$ over land and $\tau = 0.05$ over ocean that were established in section 4. Specifically, weighting the data by percentage of aerosol forcing found over land and ocean, respectively, we find that 97% of the Southern Hemisphere aerosol forcing will be above noise levels of the MODIS retrieval.

Tables 3 and 4 give the estimated uncertainties using model 2. Comparing Tables 3 and 4 to Tables 1 and 2 show little substantial difference in absolute uncertainty between choice of transport model, even when the transport models resolve different parameters and result in

different mean optical thicknesses. Model 2 has consistently lower relative errors because it has a greater mean optical thickness not because it has lower absolute error.

## 8. Cloud issues

Clouds present several difficulties. First of all, cloud contamination in the aerosol retrievals cannot be completely eliminated by cloud masking. This error contributes to the total uncertainty, but unlike the random errors presented in Tables 1–4, cloud contamination error creates a bias to higher aerosol optical thickness. In addition, even if the cloud mask perfectly eliminates cloud contamination, an opposite bias may occur. The aerosol near clouds or heavy aerosol masquerading as clouds may be thrown out by the cloud mask and ignored. These uncertainties are difficult to quantify, and at this time, without having validation for the MODIS cloud mask, we choose to do our analysis ignoring cloud mask uncertainties, rather than inventing their values. However, our results will be affected by the uncertainties we ignore.

Furthermore, the models in this study disregard cloud cover when they report the aerosol optical thickness. The models report optical thickness even in overcast conditions, when the satellites are unable to make retrievals. Figure 7 shows the mean cloud fraction for August calculated using the 11-yr International Satellite Cloud Climatology Project (ISCCP) Revised Climatological Summary Product (D2) data plotted against model-derived optical thickness. Cloud cover over the Southern Hemisphere is significant. However, the smokiest regions correspond to the least cloudy areas. Satellites will observe the majority of smoke forcing with a minimal amount of cloud interference. Furthermore, on any given day there are clear spots between clouds, and retrievals are made. Model 1 has a spatial grid of $4° \times 5°$. The MODIS spatial grid is 250–500 km, almost assuring sufficient retrievals to determine a representative mean optical thickness for every model grid square. Over the course of a month, monthly mean spatial patterns of satellite-derived aerosol should agree well with monthly mean model results, despite the different way in which clouds are handled.

## 9. Discussion and conclusions

Global distributions of aerosol optical thickness produced by transport models enable us to estimate the

TABLE 3. Uncertainty in estimating smoke aerosol forcing in the Southern Hemisphere from MODIS aerosol optical thickness using theoretical estimates of retrieval uncertainty, upper bound of background uncertainty, and model 2.

| | Optical thickness units | | | Radiative flux (W m$^{-2}$) | | | Relative error (%) | | |
|---|---|---|---|---|---|---|---|---|---|
| | Land | Ocean | SH | Land | Ocean | SH | Land | Ocean | SH |
| Background | 0.027 | 0.027 | 0.027 | 0.7 | 1.0 | 0.9 | 10 | 19 | 15 |
| Surface | 0.05 | 0.05 | 0.05 | 1.3 | 1.8 | 1.6 | 18 | 35 | 28 |
| $\tau$-dependent | 0.10 | 0.01 | 0.04 | 2.4 | 0.4 | 1.2 | 20 | 5 | 11 |
| Rmse-combined | 0.11 | 0.06 | 0.07 | 2.8 | 2.1 | 2.2 | 28 | 40 | 39 |

TABLE 4. Uncertainty in estimating smoke aerosol forcing in the Southern Hemisphere from MODIS aerosol optical thickness using empirical estimates of retrieval uncertainty, lower bound of background uncertainty, and model 2.

| | Optical thickness units | | | Radiative flux (W m$^{-2}$) | | | Relative error (%) | | |
|---|---|---|---|---|---|---|---|---|---|
| | Land | Ocean | SH | Land | Ocean | SH | Land | Ocean | SH |
| Background | 0.01 | 0.01 | 0.01 | 0.3 | 0.4 | 0.3 | 4 | 7 | 6 |
| Surface | 0.05 | 0.01 | 0.03 | 1.3 | 0.4 | 0.7 | 18 | 7 | 11 |
| $\tau$-dependent | 0.07 | 0.01 | 0.04 | 1.8 | 0.4 | 0.9 | 15 | 5 | 9 |
| Rmse-combined | 0.09 | 0.02 | 0.04 | 2.2 | 0.6 | 1.2 | 23 | 11 | 16 |

range of uncertainty we should expect from satellite remote sensing of aerosol direct forcing at the top of the atmosphere. Specifically we put the MODIS aerosol retrievals to the test and limit our study to biomass burning aerosol in the Southern Hemisphere. We want to know how much of the smoke forcing will be above the retrieval's noise level and how well we will be able to estimate the Southern Hemisphere smoke forcing.

Roughly between 85%–97% of the smoke forcing will occur in areas above noise level.

Even so, we will only be able to determine clear sky direct smoke aerosol forcing to within 1.2–2.2 W m$^{-2}$ (16%–60%) depending on the uncertainty of our retrievals. The larger uncertainty corresponds to theoretical estimates of retrieval accuracy and of background aerosol. The smaller uncertainty corresponds to estimates of retrieval accuracy based on empirical evidence from field experiments and an estimate of background aerosol based on auxiliary information. Preliminary validation of actual MODIS retrievals strongly suggests the smaller uncertainty, especially in an ensemble average over several observations.

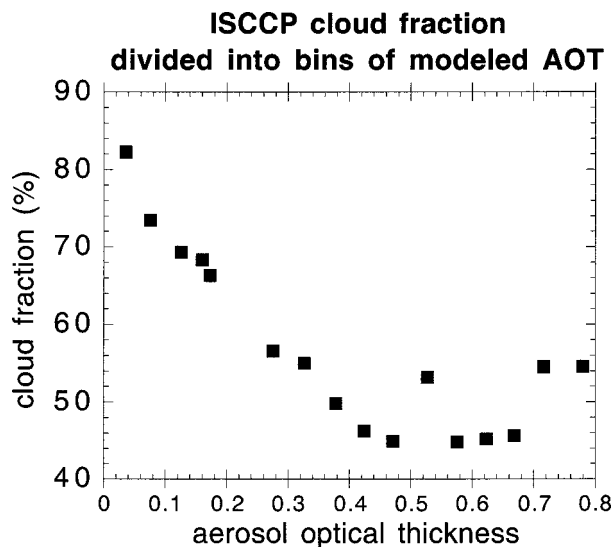## ISCCP cloud fraction divided into bins of modeled AOT



FIG. 7. Cloud fraction plotted against smoke aerosol optical thickness of the Southern Hemisphere. Cloud fraction is calculated from the ISCCP D2 11-yr mean Aug data. Smoke aerosol optical thickness values derived from the simulation of Tegen et al. (1997). Data has been sorted according to aerosol optical thickness, divided into aerosol optical thickness bins and then mean cloud fraction calculated for each bin.

Uncertainty from cloud contamination remains an unknown factor, and is not included in these calculations.

The range of absolute uncertainty appears not to be sensitive to the choice of transport model used to estimate the global distribution of smoke aerosol. However, the range of relative error does depend on the choice of transport model if one model produces a generally hazier atmosphere than the other.

How can we further reduce these uncertainties? By using satellite remote sensing to directly measure aerosol radiative fluxes rather than first retrieving aerosol optical thickness, much of the $\tau$-dependent error will be eliminated. Note that this can also be achieved by using the same aerosol optical properties to calculate the forcing as were used to retrieve the optical thickness from the satellite data (Kaufman and Tanré 2001, manuscript submitted to *J. Geophys. Res.*). However, the contribution from uncertainty in estimating background and surface reflectance remains. Just the surface uncertainties alone will account for errors of 0.7–1.6 W m$^{-2}$ (11%–48%). However, the excellent validation we are obtaining from the MODIS algorithms, both over land and ocean, strongly suggests that even the errors associated with surface assumptions are both smaller than expected and random (C01; I01; R01). Over time, these random errors of the MODIS retrievals may reduce to statistically insignificant values. Further validation efforts are needed before such a hypothesis can be verified.

In addition, a subject not explored here is the use of multiple satellite sensors working in concert to reduce uncertainties. For example, using MODIS along with the Clouds and Earth's Radiant Energy System (CERES) broadband fluxes will reduce uncertainties due to narrow to broadband conversions and multiple channel calibration issues. Still the lessons learned by this exercise apply to CERES as well. Separating smoke from background aerosol and estimating the surface contribution will remain an issue even for this broadband instrument.

In this study we have demonstrated the strengths and weaknesses of using satellite remote sensing as a tool for determining global aerosol radiative forcing at the top of the atmosphere. We see that satellites do best in regions of high aerosol loading, but the vast areas of low aerosol optical thickness introduce uncertainties in the determination. Further reduction of uncertainties calls for a strategy that utilizes a combination of satellite remote sensing with ground-based remote sensing and global transport models to reduce the uncertainty in the effects of the background aerosol and the surface re-

flective properties. Such an assimilated approach will be necessary to realize the full potential of satellite remote sensing.

## REFERENCES

Alpert, P., Y. J. Kaufman, Y. Shay-El, D. Tanré, A. da Silvas, S. Schubert, and J. H. Joseph, 1998: Quantification of dust-forced heating of the lower atmosphere . *Nature,* **395,** 367–370.

Charlson, R. J., S. E. Schwartz, J. M. Hales, R. D. Cess, J. A. Coakley Jr., J. E. Hansen, and D. J. Hofmann, 1992: Climate forcing by anthropogenic aerosol. *Science,* **255,** 423–430.

Chin, M., D. J. Jacob, G. M. Gardner, P. A. Spiro, M. Foreman-Fowler, and D. L. Savoie, 1996: A global three-dimensional model of tropospheric sulfate. *J. Geophys. Res.,* **101,** 18 667–18 690.

Chu, D. A., Y. J. Kaufman, L. A. Remer, and B. N. Holben, 1998: Remote sensing of smoke from MODIS airborne simulator during the SCAR-B experiment. *J. Geophys. Res.,* **103,** 31 979–31 988.

——, ——, C. Ichoku, L. A. Remer, D. Tanré, and B. N. Holben, 2001: Validation of MODIS aerosol optical depth over land. *Geophys. Res. Lett.,* in press.

Ghan, S. J., R. C. Easter, J. Hudson, and R.-M. Breon, 2001a: Evaluation of aerosol indirect forcing in MIRAGE. *J. Geophys. Res.,* **106,** 5317–5334.

——, and Coauthors, 2001b: A physically-based estimate of radiative forcing by anthropogenic sulfate aerosol. *J. Geophys. Res.,* **106,** 5279–5294.

——, N. Laulainen, R. Easter, R. Wagener, S. Nemesure, E. Chapman, Y. Zhang, and R. Leung, 2001c: Evaluation of aerosol direct radiative forcing in MIRAGE. *J. Geophys. Res.,* **106,** 5295–5316.

Hansen, J., M. Sato, and R. Ruedy, 1997: Radiative forcing and climate response. *J. Geophys. Res.,* **102,** 6831–6864.

Hao, W. M., M. H. Liu, and P. J. Crutzen, 1990: Estimates of annual and regional releases of $CO_2$ and other trace gases to the atmosphere from fires in the tropics, based on the FAO statistics for the period 1975–1980. *Fire in the Tropical Biota,* J. C. Goldammer, Ed., Springer-Verlag, 440–462.

Herman, J. R., P. K. Bhartia, O. Torres, C. Hsu, C. Seftor, and E. Celarier, 1997: Global distribution of UV-absorbing aerosols from Nimbus7/TOMS data. *J. Geophys. Res.,* **102,** 16 911–16 922.

Hobbs, P. V., J. S. Reid, R. A. Kotchenruther, R. J. Ferek, and R. Weiss, 1997: Direct radiative forcing by smoke from biomass burning. *Science,* **275,** 1776–1778.

Holben, B. N., and Coauthors, 1998: AERONET—A federated instrument network and data archive for aerosol characterization. *Remote Sens. Environ.,* **66,** 1–16.

Houghton, J. T., and Y. Ding, Eds., 2001: Summary for policymakers: A report of Working Group I of the Intergovernmental Panel on Climate Change. Cambridge University Press, 20 pp.

Husar, R. B., J. M. Prospero, and L. L. Stowe, 1997: Characterization of tropospheric aerosols over the oceans with the NOAA Advanced Very High Resolution Radiometer optical thickness operational product. *J. Geophys. Res.,* **102,** 16 889–16 909.

Kaufman, Y. J., D. Tanré, L. A. Remer, E. Vermote, A. Chu, and B. N. Holben, 1997a: Operational remote sensing of tropospheric aerosol over land from EOS moderate resolution imaging spectroradiometer. *J. Geophys. Res.,* **102,** 17 051–17 067.

——, A. E. Wald, L. A. Remer, B.-C. Gao, R.-R. Li, and L. Flynn, 1997b: The MODIS 2.1 $\mu$m channel—Correlation with visible reflectance for use in remote sensing of aerosol. *IEEE Trans. Geosci. Remote Sens.,* **35,** 1286–1298.

——, A. Smirnov, B. N. Holben, and O. Dubovik, 2001: Baseline maritime aerosol: Methodology to derive the optical thickness and scattering properties. *Geophys. Res. Lett.,* **28,** 3251–3254.

King, M. D., Y. J. Kaufman, D. Tanré, and T. Nakajima, 1999: Remote sensing of tropospheric aerosols from space: Past, present, and future. *Bull. Amer. Meteor. Soc.,* **80,** 2229–2259.

Lacis, A. A., and M. I. Mishchenko, 1995: Climate forcing, climate sensitivity, and climate response: A radiative modeling perspective on atmospheric aerosols. *Aerosol Forcing of Climate,* R. J. Charlson and J. Heintzenberg, Eds., John Wiley, 11–42.

Liousse, C., J. E. Penner, C. Chuang, J. J. Walton, H. Eddleman, and H. Cachier, 1996: A global three-dimensional model study of carbonaceous aerosols. *J. Geophys. Res.,* **101,** 19 411–19 432.

Martins, J. V., P. Artaxo, C. Liousse, J. S. Reid, P. V. Hobbs, and Y. J. Kaufman, 1998: Effects of black carbon content, particle size, and mixing on light absorption by aerosols from biomass burning in Brazil. *J. Geophys. Res.,* **103,** 32 041–32 050.

McGovern, F. M., F. Raes, R. V. Dingenen, and H. Maring, 1999: Anthropogenic influences on the chemical and physical properties of aerosols in the Atlantic subtropical region during July 1994 and July 1995. *J. Geophys. Res.,* **104,** 14 309–14 319.

Penner, J. E., R. E. Dickinson, and C. A. O'Neill, 1992: Effects of aerosol from biomass burning on the global radiation budget. *Science,* **256,** 1432–1434.

Perry, K. D., T. A. Cahill, R. C. Schnell, and J. M. Harris, 1999: Long-range transport of anthropogenic aerosols to the National Oceanic and Atmospheric Administration baseline station at Mauna Loa Observatory, Hawaii. *J. Geophys. Res.,* **104,** 18 521–18 534.

Prins, E. M., J. M. Feltz, W. P. Menzel, and D. E. Ward, 1998: An overview of GOES-8 diurnal fire and smoke results for SCAR-B and 1995 fire season in South America. *J. Geophys. Res.,* **103,** 31 821–31 836.

Remer, L. A., and Y. J. Kaufman, 1998: Dynamical aerosol model: Urban/industrial aerosol. *J. Geophys. Res.,* **103,** 13 859–13 871.

——, B. N. Holben, A. M. Thompson, and D. McNamara, 1998: A model of tropical biomass burning smoke aerosol size distribution. *J. Geophys. Res.,* **103,** 31 879–31 892.

——, and Coauthors, 2001: Validation of MODIS aerosol retrieval over ocean. *Geophys. Res. Lett.,* in press.

Satheesh, S. K., and V. Ramanathan, 2000: Large differences in tropical aerosol forcing at the top of the atmosphere and Earth's surface. *Nature,* **405,** 60–63.

——, ——, X. Li-Jones, J. M. Lobert, I. A. Podgorny, J. M. Prospero, B. N. Holben, and N. G. Loeb, 1999: A model for the natural and anthropogenic aerosols over the tropical Indian Ocean derived from Indian Ocean Experiment data. *J. Geophys. Res.,* **104,** 27 421–27 440.

Setzer, A. W., and M. C. Pereira, 1991: Amazonian biomass burning in 1987 and an estimate of their tropospheric emissions. *Ambio,* **20,** 19–22.

Stoller, P., and Coauthors, 1999: Measurements of atmospheric layers from the NASA DC-8 and P-3B aircraft during PEM-Tropics A. *J. Geophys. Res.,* **104,** 5745–5764.

Tanré, D., Y. J. Kaufman, M. Herman, and S. Mattoo, 1997: Remote sensing of aerosol properties over oceans using the MODIS/EOS spectral radiances. *J. Geophys. Res.,* **102,** 16 971–16 988.

——, L. A. Remer, Y. J. Kaufman, S. Mattoo, P. V. Hobbs, J. M. Livingston, P. B. Russell, and A. Smirnov, 1999: Retrieval of aerosol optical thickness and size distribution over ocean from MODIS airborne simulator during TARFOX. *J. Geophys. Res.,* **104,** 2261–2278.

——, and Coauthors, 2001: Climatology of dust aerosol size distribution and optical properties derived from remotely sensed data in the solar spectrum. *J. Geophys. Res.,* **106,** 18 205–18 218.

Tegen, I., and I. Fung, 1995: Contribution to the mineral aerosol load from land surface modification. *J. Geophys. Res.,* **100,** 18 707–18 726.

——, P. Hollrig, M. Chin, I. Fung, D. Jacob, and J. Penner, 1997: Contribution of different aerosol species to the global aerosol extinction optical thickness: Estimates from model results. *J. Geophys. Res.,* **102,** 23 895–23 915.

Twomey, S. A., 1977: The influence of pollution on the shortwave albedo of clouds. *J. Atmos. Sci.,* **34,** 1149–1152.

Walton, J. J., M. C. MacCracken, and S. J. Ghan, 1988: A global-scale Lagrangian trace species model of transport, transformation and removal processes. *J. Geophys. Res.,* **93,** 8339–8354.